Nano-impact testing of TiFeN and TiFeMoN films for dynamic toughness evaluation

B D Beake, V M Vishnyakov, J S Colligon

Nano-impact testing of TiFeN and TiFeMoN films for dynamic toughness evaluation

B.D. Beake[1,2*], V.M. Vishnyakov[2] and J.S. Colligon[2]

1 Micro Materials Ltd., Willow House, Ellice Way, Yale Business Village, Wrexham LL13 7YL, UK

2 Dalton Research Institute, Manchester Metropolitan University, Manchester M1 5GD, UK

Abstract

TiFeN and TiFeMoN films were deposited on silicon wafers by ion beam assisted deposition. Their mechanical properties were measured by nanoindentation (quasi-static) and nano-impact (dynamic) techniques. Nano-impact testing enabled assessment of their toughness and resistance to fatigue fracture under repetitive loading. At low impact forces films with a higher resistance to plastic deformation (H^3/E^2) were much more resistant to the formation of cracks throughout the test. At higher impact forces these films initially show impact resistance but with continued impacts they are unable to protect the Si substrate, performing as poorly as films with lower H^3/E^2 and suffer delamination from the Si substrate over a large area.

* Corresponding author. Tel: +44 (0) 1978 261615; Fax: +44 (0) 1978 356966. Email: ben@micromaterials.co.uk

Key words: nano-impact, nanoindentation; wear resistant coatings; thin films

1. Introduction

Industrial applications such as high speed cutting and forming processes have increasing severe mechanical contact conditions that drive the development of materials with a combination of hardness and toughness [1-2]. The optimum mechanical properties required for film toughness remain an open question. From a practical viewpoint, “super-tough” can be preferable to “super-hard” in highly loaded mechanical contact [1-2]. Nanoindentation has been used to provide an estimate of toughness [3-7]. The quantitative treatment developed by Lawn and co-workers for bulk materials [3-4] is not directly applicable to thin films as the presence of the interface influences the development of the radial crack system. For highly brittle thin films when discrete through-thickness fracture is observed in the load displacement curve (e.g. 1μm CN_x on Si) modelling may provide quantitative estimates of toughness [5-7]. However, such fracture is not observed in the load-displacement curve of tougher thin films. Chen and Bull have noted that for some coatings, even when fracture does occur, e.g. picture frame cracking of ZnO, there are no excursions on the load-displacement curves [8]. There are opposing views about how the indentation curve shape should look to correspond to a tougher material, when discontinuities (abrupt depth jumps) due to cracking are not present, and parameters such as the ratio of hardness to modulus (H/E, a measure of the partitioning between energy dissipation by elastic and plastic deformation in the indentation contact) [9-10], plasticity index (plastic work done/total work done) [11-12] and the resistance to plastic deformation (H^3/E^2) [13-20] have been investigated as these can be easily obtained in a nanoindentation test. The shape of the indentation curve itself can be considered as a “fingerprint” for a material as it is directly related to the H/E_r ratio in the contact, where E_r is the reduced indentation modulus as defined in Equation 1 (see

section 2). An increase in *H/E* results in a lower plasticity index and a more elastic contact. As an illustration nanoindentation curves for films with differing plasticity are shown in Figure 1. The plasticity index for the indentation on the softer sample (squares) is 0.48 whilst for the harder sample (circles) it is 0.31.

Toughness has been associated with minimisation of plasticity in indentation, particularly in the development of super-hard nanocomposite materials [21-22]. For hard elastic films almost complete recovery occurs in indentation and the plasticity is minimised. Musil and Jirout [16] have shown that, for indentation load up to 0.5 and 1N with a Vickers indenter, resistance to cracking is correlated with the film resistance to plastic deformation, H^3/E^2. In Figure 1 the measured H^3/E_r^2 values are 0.18 and 0.64, and, based on the Musil and Jirout analysis, the film with less plasticity would have higher resistance to cracking. The open question is whether this is beneficial in a realistic practical contact situation. When coatings are developed for highly loaded contact applications [1-3,11-12,23-28] higher plasticity in indentation has been correlated with higher toughness and durability in application conditions. Toughness is not the same as plasticity, but under highly loaded conditions cracks can propagate to failure where dissipative mechanisms such as plasticity do not exist so the two properties can be very well correlated.

In view of this apparent contradiction regarding the optimum mechanical properties for toughness, in this study a repetitive nanomechanical test has been employed to take a more direct approach to the assessment to film toughness and damage tolerance under dynamic loading. Dynamic loading represents a typical mechanical contact situation where high dynamic toughness is required to avoid coating failure problems.

The nano-impact (impulse indentation) technique in the NanoTest system can simulate the mechanical conditions occurring in contact and predict the wear performance of coated systems subjected to repetitive contact [2,29-32]. In this test repetitive high strain rate impact indentation occurs at the same location on the sample surface and the evolution of film damage can be monitored *in situ*. The test does *not* provide a direct value of the static fracture toughness K_{1c} but rather an assessment of the sample's resistance to fatigue fracture, or effective dynamic toughness, under dynamic and repetitive loading conditions that can be more representative of actual contact in applications. For example, the nano-impact test can successfully simulate the contact in extreme high speed cutting applications such as machining hard-to-cut materials with 3 μm AlCrN or TiAlN coatings deposited on cemented carbide tool inserts [2, 12]. At the start of the impact test the penetration depth is lower for the TiAlN (higher H, H/E and H^3/E^2) but as the test progresses it is more susceptible to fracture and this results in greater wear. This exactly mirrors the observed behaviour in high-speed cutting tests on hardened steel [2, 12].

In this current study we investigate the behaviour of a range of hard brittle nitride films deposited on a hard and brittle but low modulus substrate (Si wafer) under continued impact at different forces. The primary aim was to determine how the film mechanical properties influence impact resistance: (1) does increasing film H^3/E^2 increase toughness in dynamic contact? (2) are differences observed between film resistance to single impacts and prolonged repetitive impacting? (3) can the results estimate the optimum film mechanical properties necessary for improved toughness and (4) can this data help to reconcile the opposing standpoints on whether plasticity in indentation is desirable for toughness or not?

2. Experimental

The films were prepared on Si (100) wafers cleaned using the ion-assisting beam with Ar^+ ions. A dual ion beam sputtering system described in detail previously was used [38-39]. Although deposition rates are slower than in commercial PVD and CVD coating processes, the dual ion beam approach can provide the flexibility and control to deposit films with a wide range of mechanical properties [39]. Sputtering of the target was by a 1.25 keV Ar^+ ion beam and a 280-600 eV N_2^+ ion beam was used for ion-assistance of the deposited film. The sputter target comprised either (i) Ti and Fe or (ii) Ti and Fe and Mo, with the area occupied by the Fe (or Fe and Mo) determining the relative Ti-Fe(-Mo) ratio in the coating. An initial thin Ti layer was deposited first on the Si to improve adhesion and the hard coating then deposited onto this bonding layer. Nitrogen ions from the second source bombarded the growing coating during ion-assisted nitride sputtering which occurred in a nitrogen partial pressure of 1-2 x 10^{-2} Pa (see Table 1 for details). The substrate temperature was maintained constant during all the deposition steps and the film thickness was determined using an SEM. Film microstructure has been assessed by X-ray diffraction (XRD) using a Philips X'pert 20 diffractometer with Cu anode in theta-2theta configuration.

Nano-impact testing was performed using a Micro Materials NanoTest NTX fitted with a sharp cube corner diamond indenter as an impact probe. The technique has been described in detail elsewhere [2,31-37]. In addition to the repetitive impact experiments described in this current work the technique can also be used for single impacts, obtaining properties such as dynamic hardness and coefficient of restitution

[33-36]. The position of the impacting probe is recorded throughout the test in the instrument software. At the beginning of the test the surface is contacted by the impact probe under a minimum contact load (0.03 mN) to determine the depth zero. The static coil force is then applied (5-50 mN) producing elastoplastic deformation by indentation. By solenoid activation the impact probe is rapidly removed to 12 μm from the surface and then accelerated over this distance to impact the surface causing additional deformation due to the higher inertial force. Subsequent repetitive impacts every 4 seconds result in additional deformation depending on the mechanical properties of the films. The probe was accelerated at applied forces of 5-50 mN for the test duration of 300 s. The evolution of impact damage was followed in situ by probe depth vs. time plots. Abrupt increases in probe depth during the tests correspond to through-thickness cracking. Post-test microscopic analysis of impact craters confirmed through-thickness cracking and resultant film delamination. Repeat tests were performed for each sample at each load to assess any variability. The standard deviations of the initial (pre-impact) depths are within the size of the symbols in figure 4a. At 25 and 50 mN, where fracture is appreciable, the standard deviation in the final impact depth (figure 4 c) is typically in the range 10-20 %.

Nanoindentation was also performed using the Micro Materials NanoTest NTX. Multi-cycle load-controlled “load-partial-unload” experiments were performed up to 20 mN maximum load to assess the variation in mechanical properties with penetration depth. The unloading curves were analyzed using standard methods with the area function for the Berkovich diamond indenter determined by indentations into fused silica. Film-only hardness (H_{film}) was determined from the plateau (load-invariant) region and film-only reduced elastic modulus $(E_r)_{film}$ by extrapolation to

zero depth (extrapolation procedure according to ISO 14577-4) [40]. E_r is the reduced modulus defined by

$$1/ E_r = (1-\nu_s^2)/ E_s + (1-\nu_i^2)/ E_i \qquad \text{[Eqn. 1]}$$

where ν_s = Poisson's ratio for the sample, ν_i = Poisson's ratio for the diamond indenter (0.07), E_s = Young's modulus for the sample, E_i = Young's modulus for the indenter (1141 GPa). Throughout this paper for simplicity we have reported properties (such as H/E_r and H^3/E_r^2) based on E_r rather than E since E_r is directly measured in the nanoindentation test and does not require the film Poisson's ratio to be known or estimated.

3. Results

3.1 Nano-impact testing

The sample response to repetitive impact varied with film composition and impact force. As an example, the transition in failure behaviour on the $TiFe_{0.65}N_{1.45}$ film surface after impact testing for 300s at 5, 10 and 25 mN is shown in Figure 2. At 5 mN the film is resistant to cracking but localised fracture occurs at 10 mN and at 25 mN both fracture and large-area film delamination are observed.

More information can be obtained from the displacement vs. time responses during the test. Typical nano-impact behaviour at each force is shown in Figure 3. At 5 mN, the $TiFe_{0.69}N_{1.44}$ and $TiFe_{0.65}N_{1.45}$ films are resistant to cracking throughout the test and the final depth is around 500 nm (figure 3 a). The $TiFe_{0.63}N_{1.5}$ film shows the lowest impact resistance, and delamination occurs on the second impact. The

$TiFe_{0.7}N_{1.9}$ and $TiFe_{0.4}Mo_{0.4}N_2$ films show an impact behaviour between these extremes where an initial gradual increase in depth proceeds until the onset of a more marked deformation mode after 20 s for $TiFe_{0.4}Mo_{0.4}N_2$ and after 35 s for $TiFe_{0.7}N_{1.9}$. At 10 mN the $TiFe_{0.69}N_{1.44}$ and $TiFe_{0.65}N_{1.45}$ films perform well with $TiFe_{0.65}N_{1.45}$ being crack-resistant and $TiFe_{0.69}N_{1.44}$ showing only a small increase in depth after ~ 80 s (figure 3 b). For the other three films, cracking occurs almost immediately.

At 25 mN the $TiFe_{0.69}N_{1.44}$ and $TiFe_{0.65}N_{1.45}$ films are more resistant to cracking after initial impact but, upon continued impact, they fracture dramatically (figure 3 c). More extreme substrate deformation occurs at 50 mN (figure 3 d), with all films fracturing rapidly and unable to protect the substrate from further damage. Final probe depths were in the range 5-10 μm.

Key parameters in the impact test are summarised in figure 4 a-d. These are

(1) probe depth prior to initial impact

(2) probe depth after first impact

(3) final impact probe depth

(4) increase in probe depth due to continued impact (i.e. the difference in depth between 3 and 2 above)

3.2 Nanoindentation

Table 1 summarises the mechanical properties of the films determined by load-partial unload nanoindentation. Values of film elastic modulus independent of substrate influence were obtained by a linear extrapolation to zero-depth. Film hardness varied from 16-24 GPa. With H_{film} and $E_{r,,film}$ known it was possible to determine film-only

values of $(H/E_r)_{film}$ and $(H^3/E_r^2)_{film}$ (Table 1). The harder films showed enhanced stiffness but the value of $(H/E_r)_{film}$ covered a relatively small range (0.083-0.093). Film thickness varied between 0.7 and 1.7 μm. More marked differences were found in the parameter $(H^3/E_r^2)_{film}$, a measure of the film-only resistance to plastic deformation which varied between 0.11 for the softest film and 0.21 for the hardest. Figure 5 shows how the resistance to plastic deformation in the contact varies with increasing penetration into the films. Although the value of H^3/E_r^2 in the contact varies with penetration depth (primarily due to the increased contribution from the much lower modulus Si substrate), the data clearly show that $TiFe_{0.69}N_{1.44}$ and $TiFe_{0.65}N_{1.45}$ films are significantly more resistant to plastic deformation.

3.3 Microstructural analysis

Figure 6 shows the XRD spectra of the films. In conjunction with ion assistance, the high N_2 partial pressure during deposition of $TiFe_{0.69}N_{1.44}$ and $TiFe_{0.63}N_{1.5}$ resulted in fully amorphous films whilst the $TiFe_{0.69}N_{1.44}$ and $TiFe_{0.7}N_{1.9}$ deposited under lower N_2 partial pressure shows peak in their XRD spectra. The $TiFe_{0.4}Mo_{0.4}N_2$ film was amorphous.

4. Discussion

The films are compositionally different from $Ti(Fe)N_x$ films deposited by Musil and co-workers who reported that, when the Fe content was sufficiently low (≤15 at.%), single-phase nanocomposite films could be obtained with hardness up to 45 GPa [14]. Our films contain a much higher % Fe and are softer due to FeN formation. The XRD analysis has shown that the TiFeN film structure is controlled by both the nitrogen partial pressure and the presence of ion assistance. At high nitrogen partial pressure

ion assistance produces fully amorphous TiFeN films as the temperature of the substrate is not high enough to recrystallise them. The $TiFe_{0.4}Mo_{0.4}N_2$ film is also amorphous, presumably as with more elements it is unlikely to be crystalline.

At ~20 GPa the TiFeN and TiFeMoN films have similar hardness to thin films (such as a-C, nc-TiC/a-C, TiC/a-C, TiC/a-C:H, nc-TiC/a-C(Al), YSZ/Au) reported to have excellent toughness [17-18,23-25,28] and high plasticity in indentation. The resistance to plastic deformation H^3/E^2 and the partitioning between energy dissipation by elastic and plastic deformation H/E are well correlated for these thin films. Musil and co-workers have shown that nanocomposite films with higher hardness also tend to have higher H^3/E^2 [13-16] and this is consistent with the results in Table 1. In what follows the discussion has been based around H^3/E_r^2 for convenience but Table 1 shows that similar arguments also apply for H/E_r.

Nanoindentation can be used to assess resistance to crack initiation and overload failure but it is not possible to monitor crack propagation under repetitive, oscillating loading conditions in the conventional quasi-static test. The dynamic nano-impact test is a complementary technique that can determine the resistance of the film-substrate system to fatigue fracture, i.e. the formation and propagation of cracks under repetitive loading. Tougher films with plastic deformation and micro-cracking mechanisms appear beneficial in minimising large-area delamination under these conditions. The abrupt increases in impact probe depth (such as those observed in Figures 3(a), (b) and (c) after 6 s at 10 mN on $TiFe_{0.4}Mo_{0.4}N_2$, $TiFe_{0.7}N_{1.9}$ and $TiFe_{0.63}N_{1.5}$) are due to fracture. With a NanoTest modified for fast data acquisition up to 200 kHz, Jennett and Nunn recently reported [37] a dramatic reduction in

rebound height for impacts which result in fracture (due to the enhanced energy absorbed in the creation of the free surfaces) and also that these impacts have a direct correspondence with the observed depth steps.

It is clear from figure 3 that mechanical properties have an important influence on durability to repetitive impact, consistent with previous studies of thin film systems [1-2, 29-31]. Results at lower load (figure 3 a-b) are consistent with $TiFe_{0.69}N_{1.44}$ and $TiFe_{0.65}N_{1.45}$, the harder films with highest H^3/E_r^2 of ~0.2 being able to provide effective load-support and protecting the silicon substrate throughout the nano-impact test. This is sufficient to avoid cracking at 5 mN but lead to the propagation of small cracks causing total failure at 10 mN.

Examination of the data presented by Pei and co-workers shows that the onset critical load for indentation-induced radial cracking with a cube corner indenter correlates well with H^3/E^2 for a range of 1.5 μm nc-TiC/a-C:H films [17]. Musil and co-workers have reported that H^3/E_r^2 and film thickness both influence cracking resistance in microindentation with a Vickers indenter, with thicker and higher H^3/E_r^2 films being more resistant [16]. The low thickness of $TiFe_{0.63}N_{1.5}$ and $TiFe_{0.7}N_{1.9}$ films may be a factor in their low crack resistance at 5 and 10 mN. The onset of circular cracking has been correlated with the ratio of indentation depth to film thickness by Musil and co-workers in microindentation [16]. In the current study the sputtering effect at high ion assistance results in more intense ion bombardment and smaller film thickness. At 700 nm, $TiFe_{0.63}N_{1.5}$ is the thinnest of all the films and fractures immediately at 5 mN. But film thickness is not the sole factor since one of the thickest films, $TiFe_{0.4}Mo_{0.4}N_2$, also fractures at low load. Thickness has been shown previously to

affect the nano-impact response of 2.3-4.5 μm a-C:H films on at low load (5 mN, cube corner indenter). Thicker a-C:H films showed more damage tolerance, providing load support for the substrate even after some cohesive fracture, although there was little effect on the number of impacts required for cohesive fracture. In general, film thickness has been found to influence nano-impact behaviour to a much smaller extent than nano-scratch testing. For example, critical loads for film failure in nano-scratching ta-C films on Si and a-C:H-based films on glass scale with film thickness [41-42] but the number of impacts required for failure can show an opposite trend. In nano-impact tests at low load (5 mN, cube corner indenter) a 140 nm a-C:H with H^3/E_r^2 = 0.21 required almost twice as many impacts to fail as a 600 nm Si-doped a-C:H with H^3/E_r^2 = 0.16.

The impact results at 25 and 50 mN applied load (fig. 3 c-d) do not show the same correlation with the mechanical properties of the films observed at lower load. As the impact force increases the enhanced load support provided by the higher H^3/E_r^2 films is no longer sufficient to protect the substrate from deformation and causes film fracture and increasing impact-induced damage throughout the test. A sharp decrease in film durability with increasing applied load in the nano-impact test has been reported previously for 2.3 μm a-C:H/Cr on steel with H^3/E_r^2 = 0.21 [30]. At low load this coating was relatively durable. It showed only small cohesive fractures after long impact times but, above a threshold load of 10 mN, through-thickness cracking led to complete removal of the coating soon after the start of the test. Bousser and co-workers have shown that for 8-13 μm CrN and CrSiN films on stainless steel the ratio of indentation depth to film thickness (d/h) at which circular cracking in Vickers indentation occurs was correlated with plasticity and *inversely* correlated with H^3/E_r^2,

suggesting that, under these highly loaded conditions, the inability of the coating to accommodate the substrate deformation drives the cracking process [19].

From individual impact depth vs. time graphs (as in figure 3) it is possible to separate film behaviour into three distinct regimes as the test progresses: (i) load support (pre-impact) (ii) initial impact and (iii) subsequent impacts. This procedure enables the role of film properties on load-support, initial resistance to crack nucleation and subsequent crack propagation to be investigated in more detail. In figure 4 the data for two films with very high H^3/E_r^2, (dotted lines) have been contrasted with the data for films with lower H^3/E_r^2, (full lines). The initial load-support prior to impact is greater for these two films throughout the load range (fig 4(a)). The probe depth after a single impact shows a similar trend (fig 4(b)). It is an appreciable fraction of the film thickness even at low load. Figure 4 (c) shows that the increase in depth due to repetitive impact (i.e. final depth – depth after initial impact) varies with load. At low load this increase is smaller for the two TiFeN films with higher H^3/E_r^2, since these do not fracture on repetitive impact. However, comparison of figures 4 (b) and (c) shows that, although resistance to single impact is improved by increasing H^3/E_r^2, durability at high dynamic contact load is not. At lower impact load, the ratio of impact depth to film thickness is low so higher H^3/E_r^2, in the film is beneficial by preventing cracks from forming in the first place. Increasing H^3/E_r^2, has been associated with high resistance to cracking and hence high fracture toughness [13-20]. At higher impact load, effective durability and damage tolerance requires resistance to both formation *and* propagation of cracks under dynamic loading. For Vickers indentation, it has been reported that cracks often form when d/h > 0.5 [19], so it is reasonable to assume cracks form on first impact at higher load, and the subsequent film behaviour in

figures 3c and 3d is the response of increasingly cracked films to continued impacts. The two TiFeN films with higher H^3/E_r^2, have better *initial* impact resistance but as the test continues fracture occurs progressively and they are unable to protect the substrate from deformation. The brittle films cannot accommodate this deformation and tensile stresses arise causing film cracking leading to the dramatic delamination failure (as observed in figure 2). Dissipative mechanisms such as plastic deformation and micro-cracking may be beneficial in relieving accumulated strain for the films with lower H^3/E_r^2. Large area delamination occurs in nano-scratch testing due to tensile stress accumulation on high H^3/E^2 TiFeN and nc-TiN/a-Si_3N_4 nanocomposites deposited on silicon [43] but is absent on films with lower hardness and H^3/E^2. Zhang and co-workers have shown that the durability nc-TiN/a-Si_3N_4 nanocomposites in scratch tests was enhanced at hardness ~20 GPa, gradually decreasing as hardness approached 40 GPa [26].

The apparent disparity in the literature reports relating the shape of the indentation load-displacement curve to film toughness may well relate to the severity of the contact conditions under which toughness is assessed. Plasticity can provide a reasonable first estimate of toughness in the engineering sense as plasticity is related to fracture resistance. Fox-Rabinovich and co-workers have shown that the optimum mechanical properties for fracture resistance and tool life in cutting tool coatings depends strongly on the type of cutting test [11]. At low load where fracture is less likely, improving film wear resistance by minimising plasticity is more important. Substrate deformation can then be prevented by the coating having a high H^3/E^2 value so that cracking is minimised. Although the TiFeN films possess no intrinsic resistance to high load impact when deposited on the brittle and low modulus Si

substrate, they may yet have the potential to be used on higher modulus substrates, with bias-grading for stress-relief. Ma and co-workers have shown that wear resistance of nc-TiN/a-Si_3N_4 in pin-on-disk tests is improved by high hardness [22]. Film deposition with graded interface layers between the substrate and the composite coatings has also been shown to enhance the scratch test critical load and relieve interface stresses [24]. Guruvenket and co-workers have recently reported that surface nitriding of low alloy steel substrates prior to deposition of nc-TiN/a-SiN_x and nc-TiCN/a-SiCN films produced a more gradual change in hardness from substrate to film and reduced the interfacial stress resulting in excellent wear resistance when sliding against 6 mm alumina balls [20].

With appropriate tuning of deposition conditions many nanocomposite thin film systems such as a-C, TiC/a-C, TiC/a-C:H, nc-TiC/a-C(Al), YSZ/Au, TiFeN and nc-TiN/a-Si_3N_4 can have the combination of (1) high plasticity in indentation (2) high toughness in applications and (3) H ~15-20 GPa. Dissipative mechanisms such as grain boundary sliding, which is possible due to this moderate hardness, result in high toughness and resistance to extreme cracking at high contact load. Suppressing dislocation activity to produce harder and super-hard films may be detrimental to their durability under highly loaded conditions, particularly if these films are deposited on softer and more compliant substrates.

5. Conclusions

The resistance to fatigue fracture by nano-impact testing enables an assessment of the relative toughness of TiFeN films on silicon under dynamic loading. From individual impact depth vs. time graphs it has been shown that film behaviour can be assessed

during three distinct regimes as the test progresses: (i) load support (pre-impact) (ii) resistance to a single (initial) impact and (iii) resistance to subsequent impacts. Film behaviour varies dramatically as a function of impact force and number of impacts. The resistance to a single (initial) impact was always improved by increasing the films' resistance to plastic deformation (H^3/E^2), as determined by nanoindentation. On repetitive impacting at low forces films with a higher resistance to plastic deformation were much more resistant to the formation of cracks. However, as the impact force in the test increased these films cracked, behaved no better than films with lower hardness and H^3/E^2 and subsequently suffer delamination over a large area. The optimum mechanical properties for improved dynamic toughness therefore depend on the severity of the impact conditions. Suppressing dislocation activity to produce yet harder films (very high H^3/E^2) is beneficial for low load contacts but can be detrimental to their durability under highly loaded contacts as suitable dissipative mechanisms are not available.

6. Acknowledgements

Dr O. Crisan is gratefully acknowledged for performing the XRD analysis.

7. References

1. Physical and Mechanical Properties to characterize Tribological Compatibility of Heavy Loaded Tribo-systems (HLTS), G.S. Fox-Rabinovich, L.S. Shuster, B.D. Beake, S.C. Veldhuis, pp121-150, In: Self-organization during friction: Advanced surface engineered materials and systems design, G.S. Fox-Rabinovich, G. Totten (eds.) Taylor and Francis Books/ CRC Press LLC, 2007.

2. Using nanomechanics to optimise coatings for cutting tools B.D. Beake, S.R. Goodes, J.F. Smith, G.S. Fox-Rabinovich and SC Veldhuis, in Handbook of Nanostructured Thin Films and Coatings, Mechanical Properties, Chapter 6, pp205-244, Ed. S Zhang, CRC Press, Taylor and Francis Group, USA (2010).
3. B.R. Lawn, A.G. Evans and D.B. Marshall, J. Am. Ceram. Soc. 63, (1980) 574.
4. G.R. Anstis, P. Chantikul, B.R. Lawn and D. B. Marshall, J. Am. Ceram. Soc., 64 (1981) 533.
5. J. den Toonder, J. Malzbender, G. de With and R. Balkenenede, J. Mater. Res. 17 (2002) 224.
6. J. Chen and S.J. Bull, Tribology 2 (2008) 219.
7. J. Chen and S.J. Bull, Thin Solid Films 517 (2009) 2945.
8. J. Chen and S.J. Bull, J. Phys. D: Appl. Phys 40 (2007) 5401.
9. A. Leyland and A. Matthews, Wear 246, 1 (2000).
10. A. Leyland and A. Matthews, Surf. Coat. Technol., 177-178 (2004) 317.
11. G.S. Fox-Rabinovich, S.C. Veldhuis, V.N. Scvorstov, L.S. Shuster, G.K. Dosbaeva, Thin Solid Films, 469-470 (2004) 505.
12. B.D. Beake, G.S. Fox-Rabinovich, S.C. Veldhuis and S.R. Goodes Surf. Coat. Technol. 203 (2009) 1919.
13. J. Musil, F. Kunc, H. Zeman and H. Polakova, Surf. Coat. Technol. 154 (2002) 304.
14. J. Musil, H. Polakova, J. Suna and J. Vlcek, Surf. Coat. Technol. 177-178 (2004) 289.
15. J. Musil, pp407-463 in Nanostructured coatings, Eds. A. Cavaleiro and J. Th. M. De Hosson, Springer, New York 2006.

16. J. Musil and M. Jirout, Surf. Coat. Technol. 201 (2007) 5148.

17. Y.T. Pei, D. Galvan and J.Th.M. De Hosson, Acta Materialia 53 (2005) 4505.

18. D. Galvan, Y.T. Pei and J.Th.M. De Hosson, Surf. Coat. Technol. 200 (2006) 6718.

19. E. Bousser, M. Benkahoul, L. Martinu and J.E. Klemberg-Sapieha, Surf. Coat. Technol. 203 (2008) 776.

20. S. Guruvenket, D. Li, J.E. Klemberg-Sapieha, L. Martinu and J. Szpunar, Surf. Coat. Technol. 203 (2009) 2905.

21. S. Veprek, J. Vac. Sci. Technol. A 17 (1999) 2401.

22. S. Ma, J. Prochazka, P. Karvankova, Q. Ma, X. Niu, X. Wang, D. Ma, K. Xu and S. Veprek, Surf. Coat. Technol. 194 (2005) 143.

23. A.A. Voevodin, J.J. Hu, J.G. Jones, T.A. Fitz and J.S. Zabinski, Thin Solid Films 410 (2001) 187.

24. A.A. Voevodin and J.S. Zabinski, Comp. Sci. Technol. 65 (2005) 741.

25. S. Zhang, X.L. Bui, Y. Fu and H. Du, Int. J. Nanoscience 3 (2004) 571.

26. S. Zhang, X.L. Bui, X.T. Xeng and X. Li, Thin Solid Films 482 (2005) 138.

27. S. Zhang, D. Sun, Y. Fu and H. Du, Surf. Coat. Technol. 167 (2003) 113.

28. S. Zhang, X.L. Bui, Y. Fu, D.L. Butler and H. Du, Diamond Relat. Mater. 13 (2004) 867.

29. B.D. Beake and J.F. Smith, Surf. Coat. Technol. 188-189C (2004) 594.

30. B.D. Beake, Surf. Coat. Technol. 198 (2005) 90.

31. B.D. Beake, G.A. Bell, S.R. Goodes, N.J. Pickford and J.F. Smith, Surf. Eng. 26 (2010) 37.

32. G.Constantinides, C.A. Tweedie, D.M. Holbrook, P. Barragan, J.F. Smith and K.J. Van Vliet, Mater. Sci. Eng. A 489 (2008) 403.

33. G.Constantinides, C.A. Tweedie, N. Savva, J.F. Smith and K.J. Van Vliet, Exp. Mech. 49 (2009) 511.
34. J.R. Trelewicz and C.A. Schuh, Appl. Phys. Lett. 93 (2008) 1717916.
35. Z.I. Kalcioglu, M.Qu, K.E. Strawhecker, T. Shazly, E. Edelman, M.R. VanLandingham, J.F. Smith and K.J. Van Vliet, Phil. Mag. 2010 iFirst.
36. J.M. Wheeler, C.A. Collier, J.M. Paillard and J.A. Curran, Surf. Coat. Technol. 204 (2010) 3399.
37. N.M. Jennett and J. Nunn, Phil. Mag. 2010 iFirst.
38. J.S. Colligon, V. Vishnyakov, R. Valizadeh, S.E. Donnelly and S. Kumashiro, Thin Solid Films 485 (2005) 148.
39. J.S. Colligon, Phil. Trans. R. Soc. Lond. A 362 (2004) 103.
40. ISO 14577: Metallic Materials – Instrumented Indentation Test for Hardness and Materials Parameters, Part 4 - Test Method for metallic and non-metallic coatings.
41. B.D. Beake, S.R. Goodes and B. Shi, J Phys D: Appl Phys 42 (2009) 065301.
42. B.D. Beake, A.A. Ogwu and T. Wagner Mater Sci Eng A 423 (2006) 70.
43. B.D. Beake, V.M. Vishnyakov, R. Valizadeh and J.S. Colligon, J. Phys. D: Appl. Phys 39 (2006) 1392.

Table 1 Composition and mechanical properties of TiFeN and TiFeMoN films

Composition	Ion Assist/V	pN_2 (Pa)	Thickness (nm)	H (GPa)	E_r (GPa)	H/E_r	H^3/E_r^2 (GPa)
$TiFe_{0.69}N_{1.44}$	280	0.011	1700	23.7	254	0.093	0.206
$TiFe_{0.65}N_{1.45}$	300	0.011	1400	22.3	241	0.093	0.191
$TiFe_{0.4}Mo_{0.4}N_2$	-	0.011	~1650	19.8	220	0.090	0.160
$TiFe_{0.63}N_{1.5}$	600	0.021	700	20.0	240	0.083	0.139
$TiFe_{0.7}N_{1.9}$	600	0.021	920	16.0	192	0.083	0.111

In Table 1 the values of *H, E, H/E_r and H^3/E_r^2* are all *film-only* properties determined from load-partial unload nanoindentation tests. Film hardness was determined from the plateau (load-invariant) region and film elastic modulus by extrapolation to zero depth.

Figure captions

1. Nanoindentation curves for films with high (squares) and low (circles) plasticity. The regions corresponding to the plastic (W_{pl}) and elastic work (W_{el}) are shown for the high plasticity sample.

2. Optical micrograph of $TiFe_{0.65}N_{1.45}$ film surface after impact tests at 5 mN (left), 10 mN (middle) and 25 mN (right).

3. Illustrative impact depth vs. time graphs for the nanocomposite films at 5-50 mN coil force. (a) 5 mN (b) 10 mN (c) 25 mN (d) 50 mN. Key:- $TiFe_{0.63}N_{1.5}$ = circles; $TiFe_{0.69}N_{1.44}$ = crosses; $TiFe_{0.65}N_{1.45}$ = squares; $TiFe_{0.7}N_{1.9}$ = diamonds; $TiFe_{0.4}Mo_{0.4}N_2$ = triangles.

4. Mean values of (a) Probe depth prior to initial impact (b) Probe depth after first impact (c) Increase in probe depth due to continued impact; i.e. [depth (final) – depth (after first impact)]. (d) Final impact depth. The key for 4 (a-d) is as in figure 3.

5. Variation in measured H^3/E_r^2 (film and substrate composite response) with increasing depth from multi-cycle (load partial unload) nanoindentation to 20 mN.

6. XRD spectra of films.

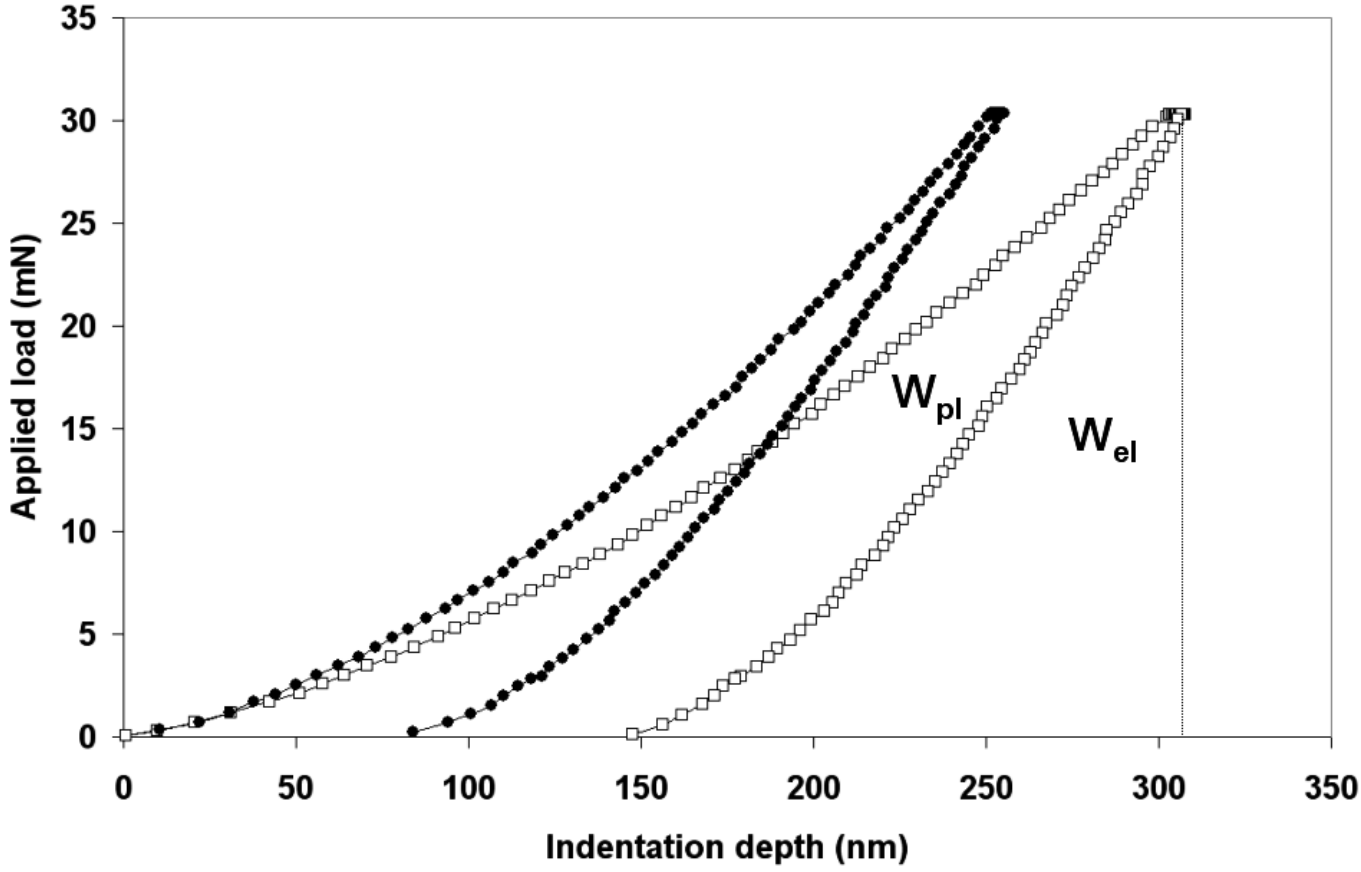

Figure 1 (fig1.tif)

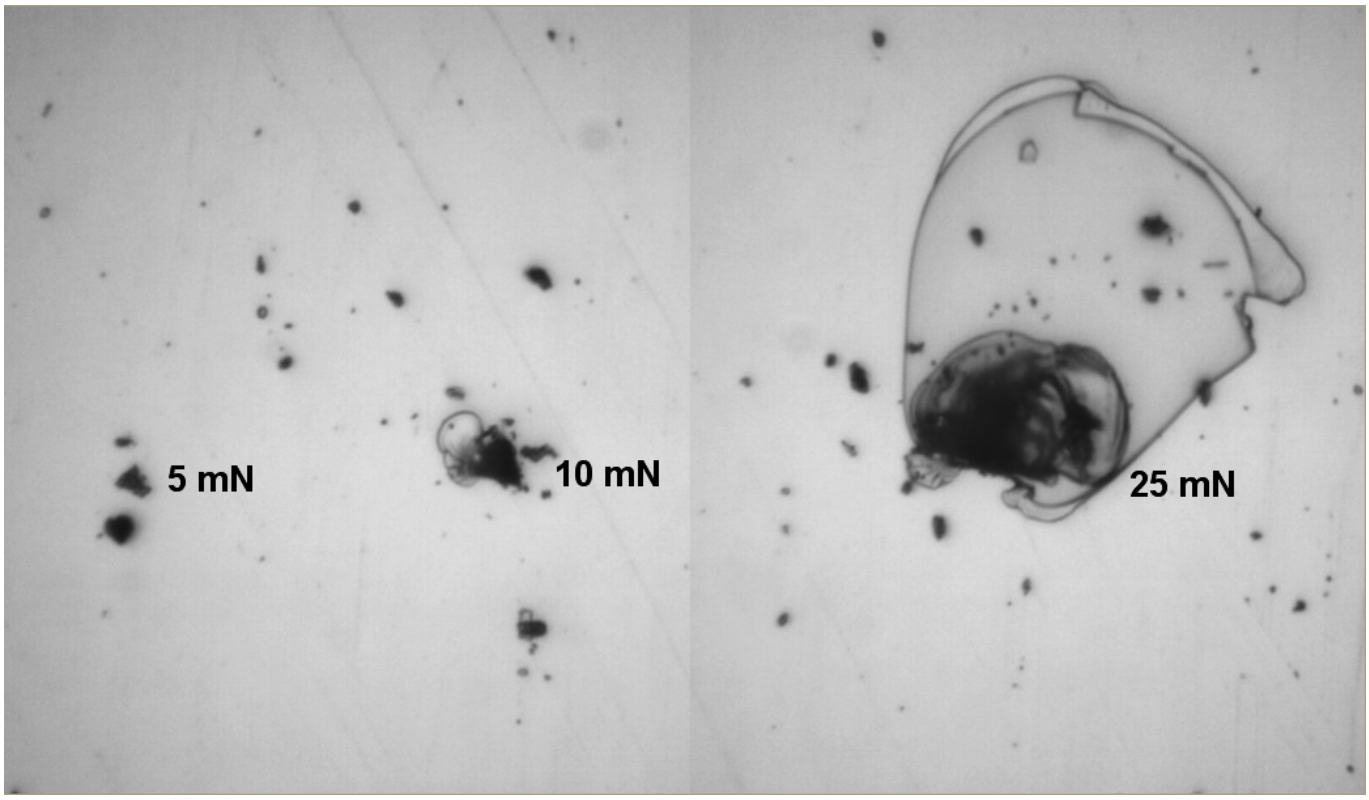

Figure 2 (fig2 NEW.tif)

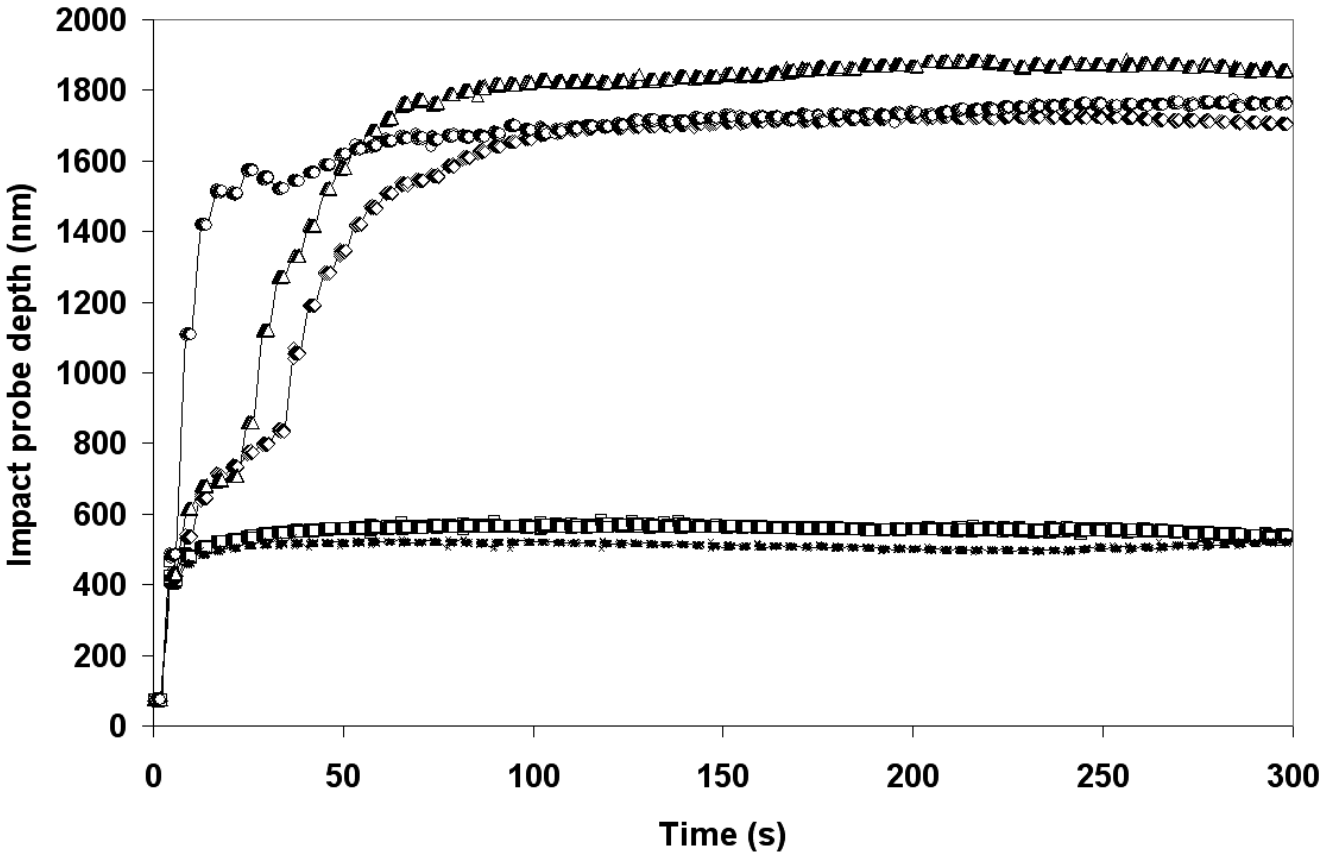

Figure 3a (fig3a 5mN.tif)

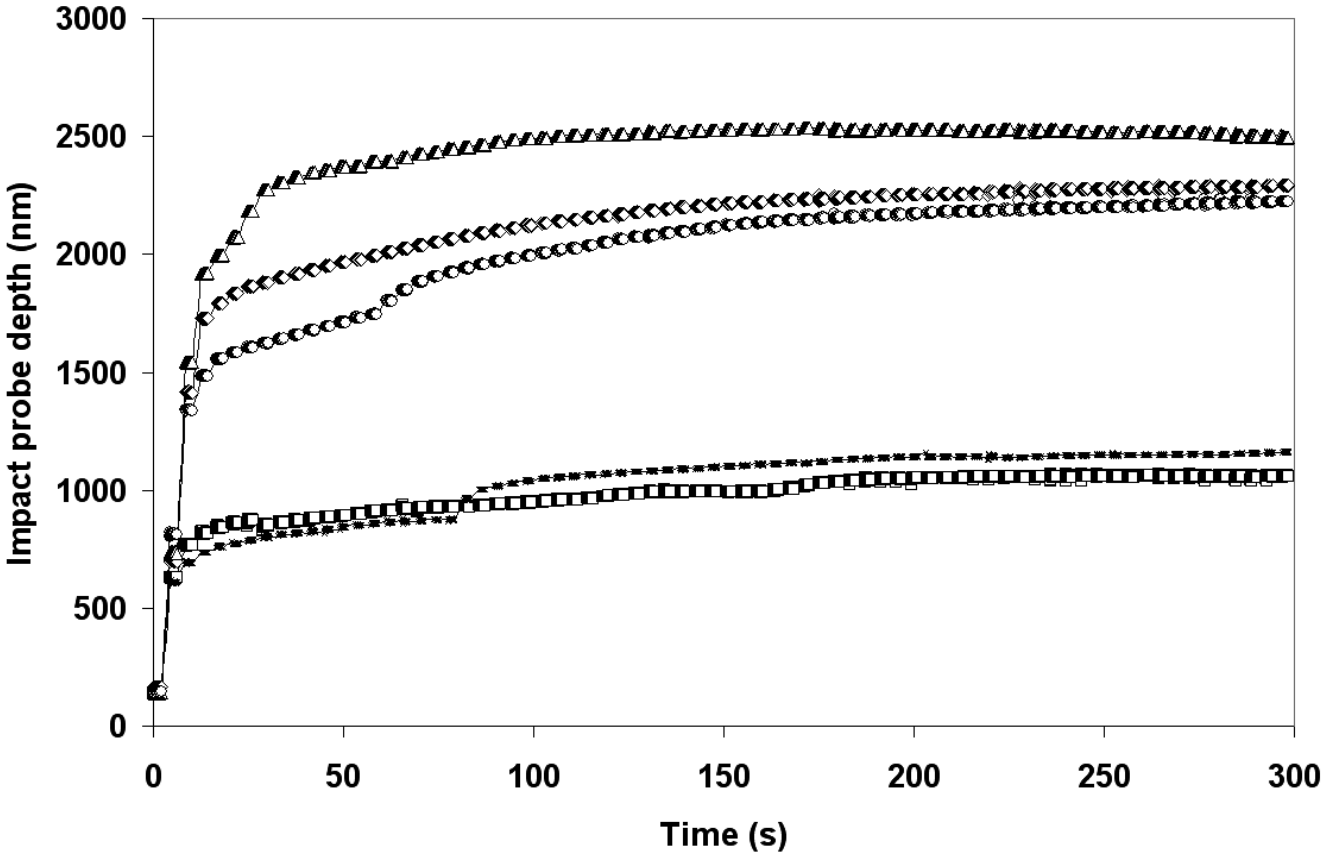

Figure 3b (fig3b 10mN.tif)

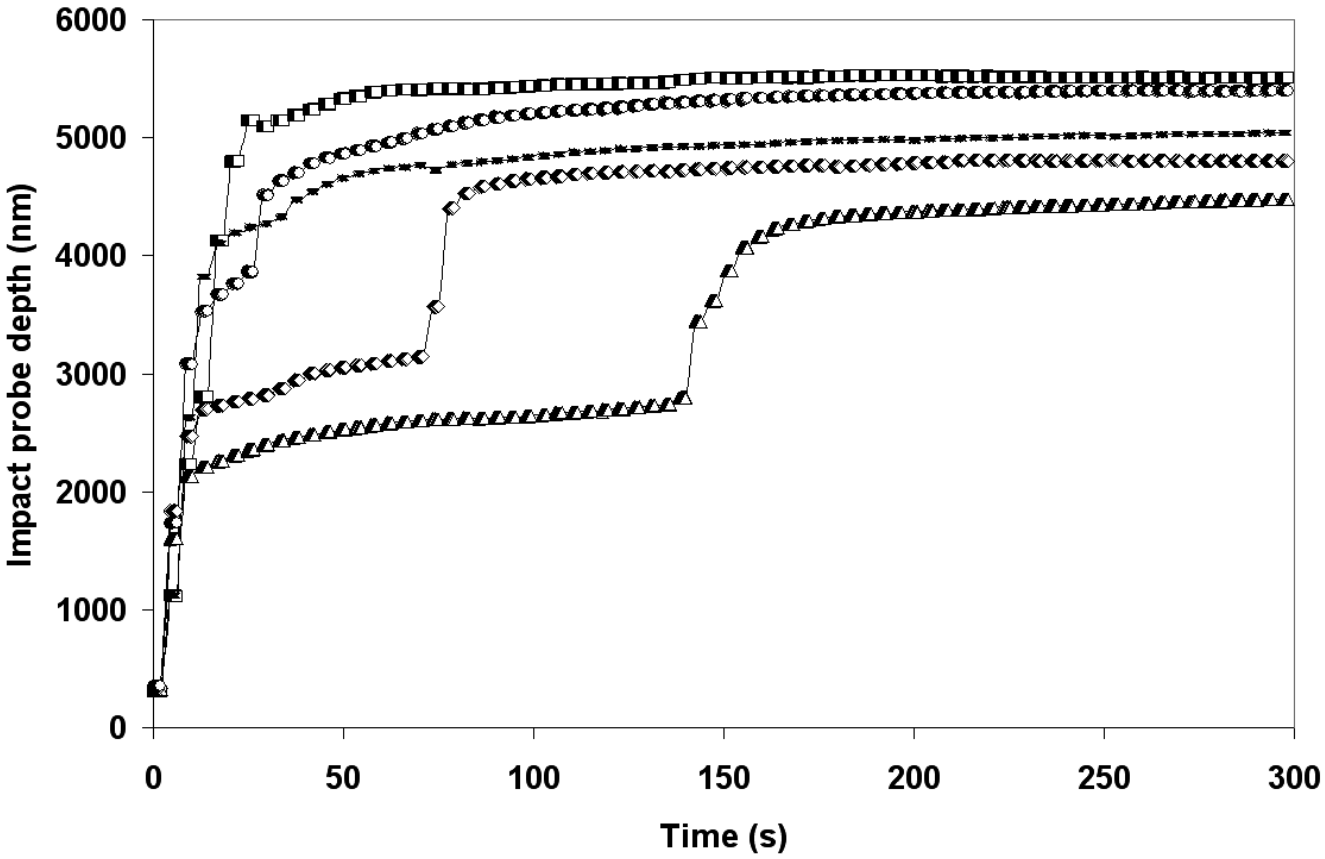

Figure 3c (fig3c 25mN.tif)

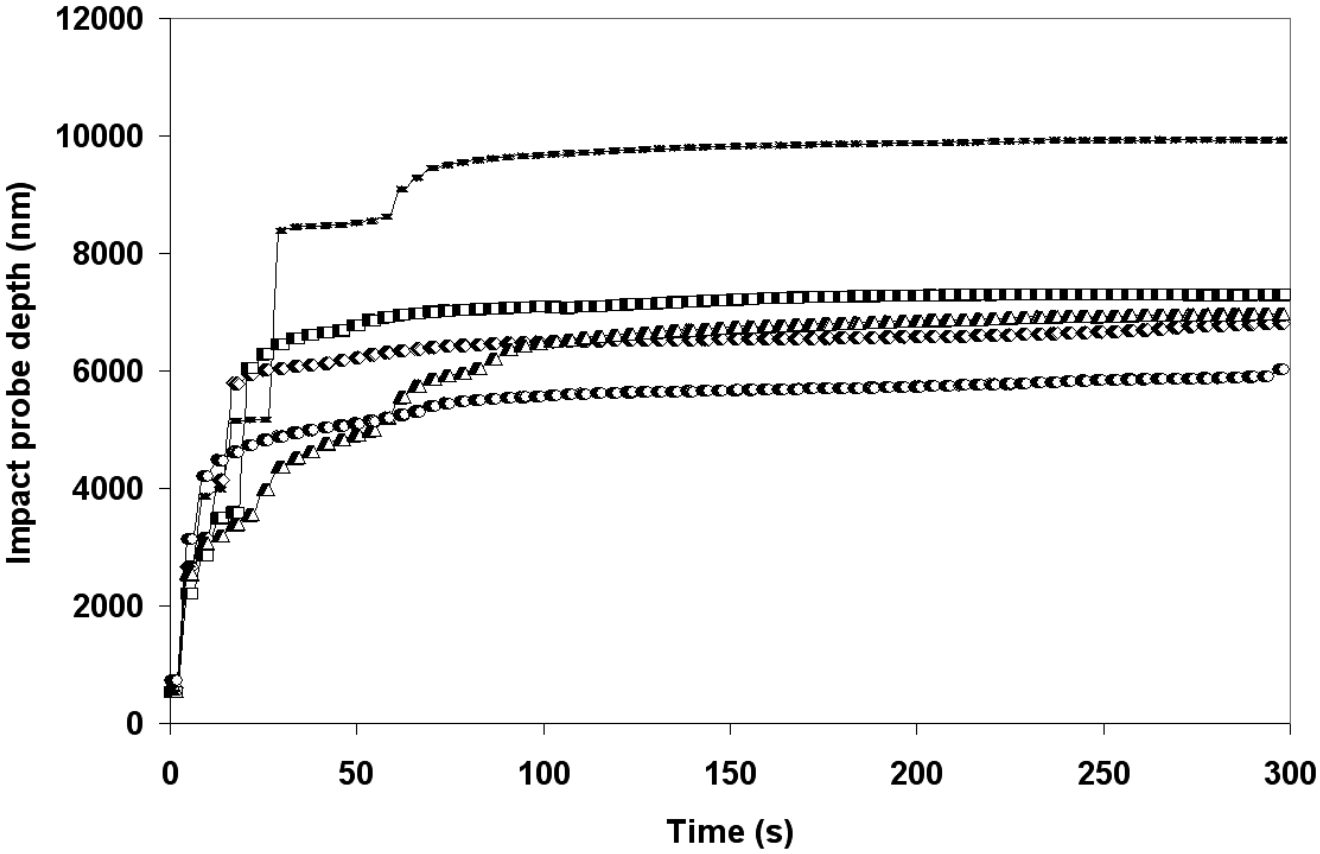

Figure 3d (fig3d 50mN.tif)

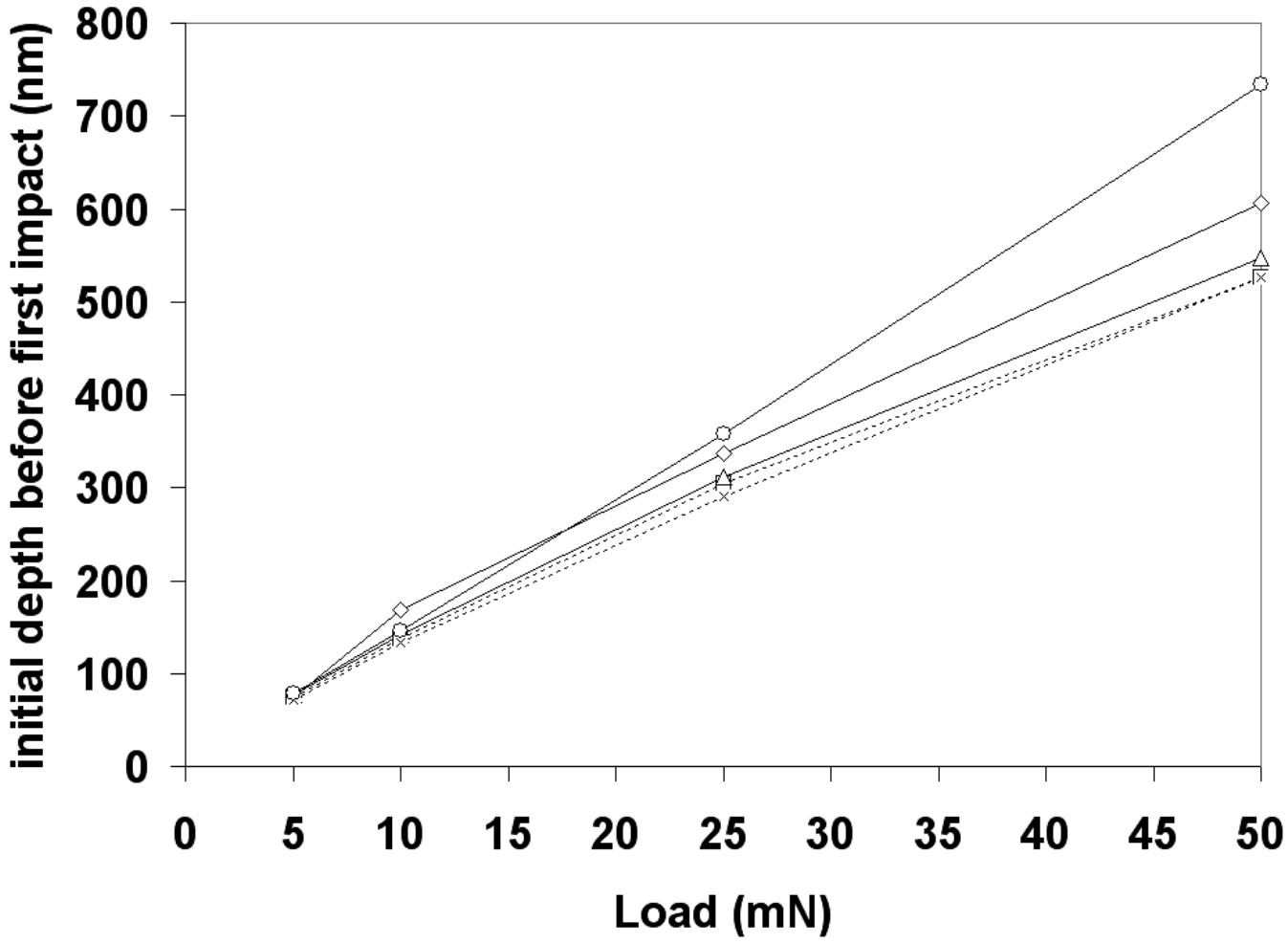

Figure 4a (fig4a.tif)

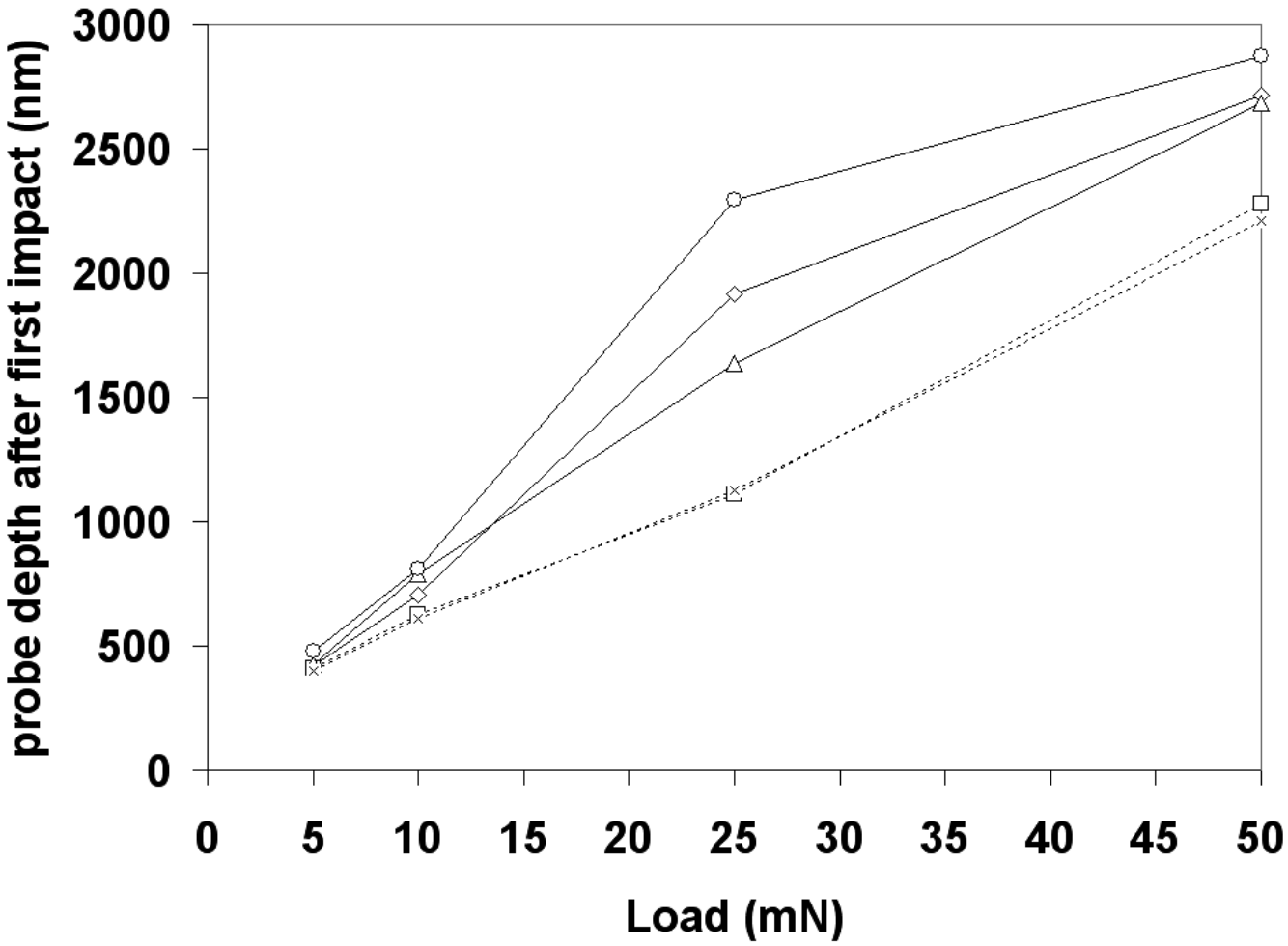

Figure 4b (fig4b.tif)

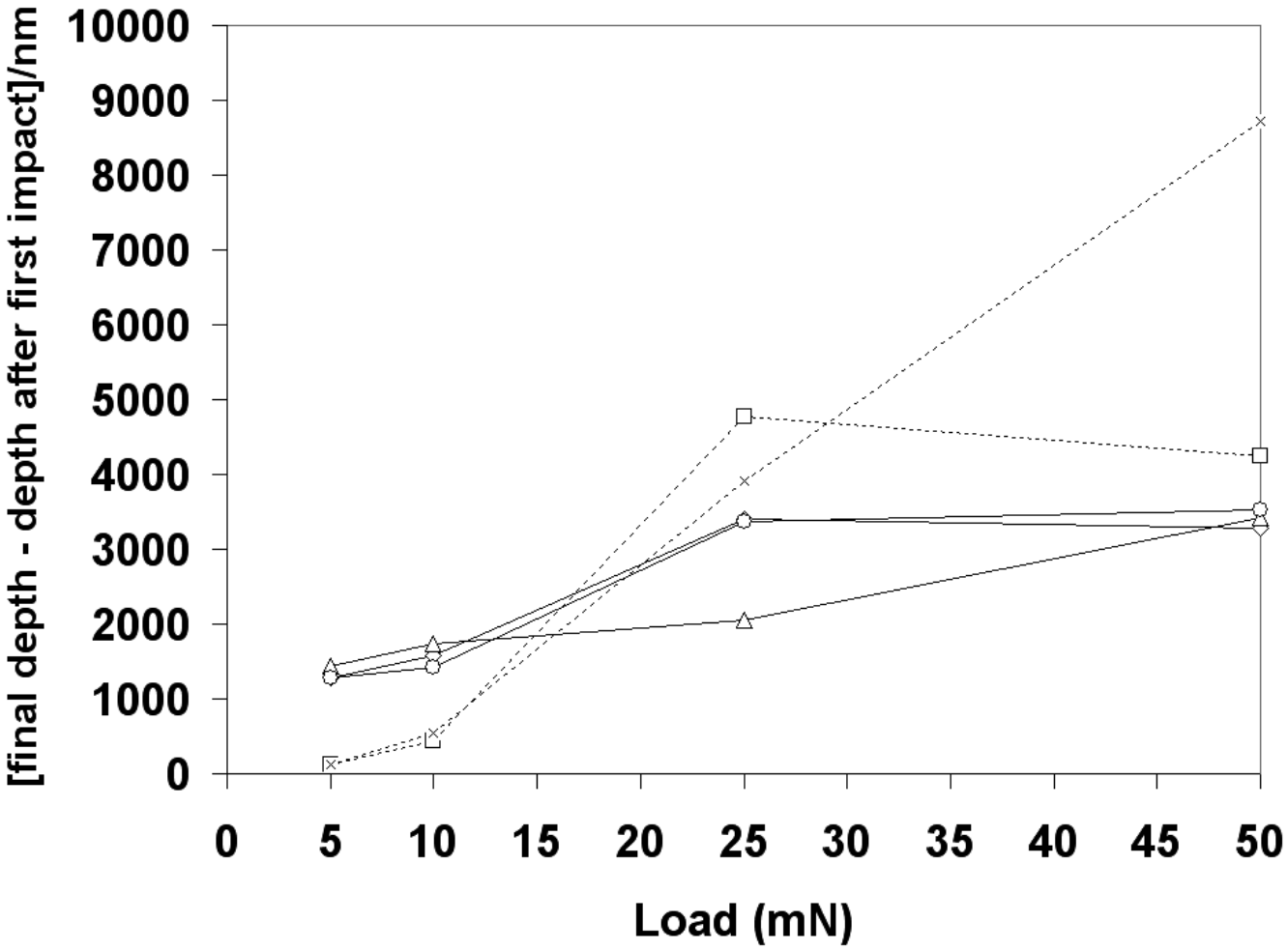

Figure 4c (fig4c.tif)

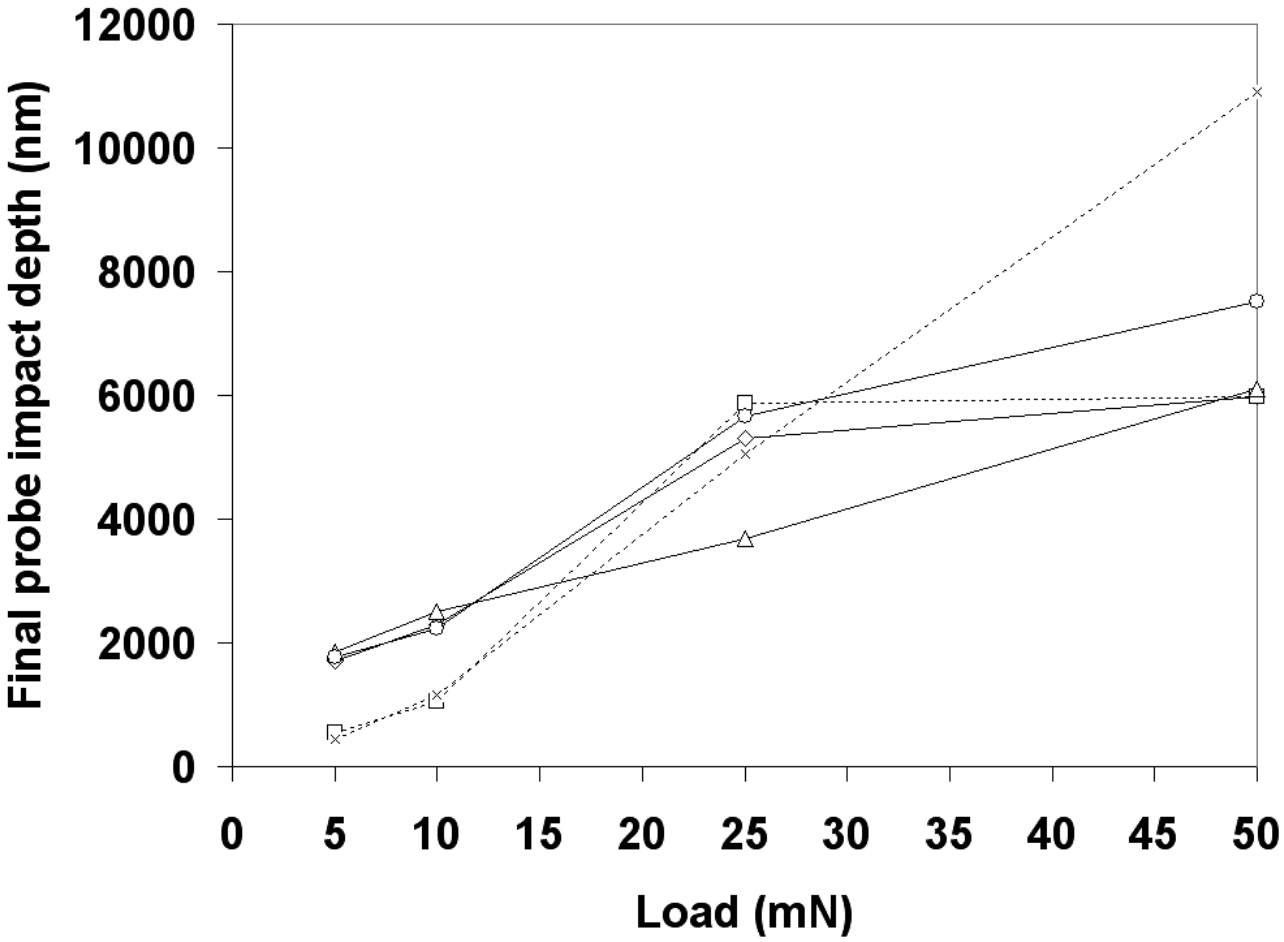

Figure 4d (fig4d.tif)

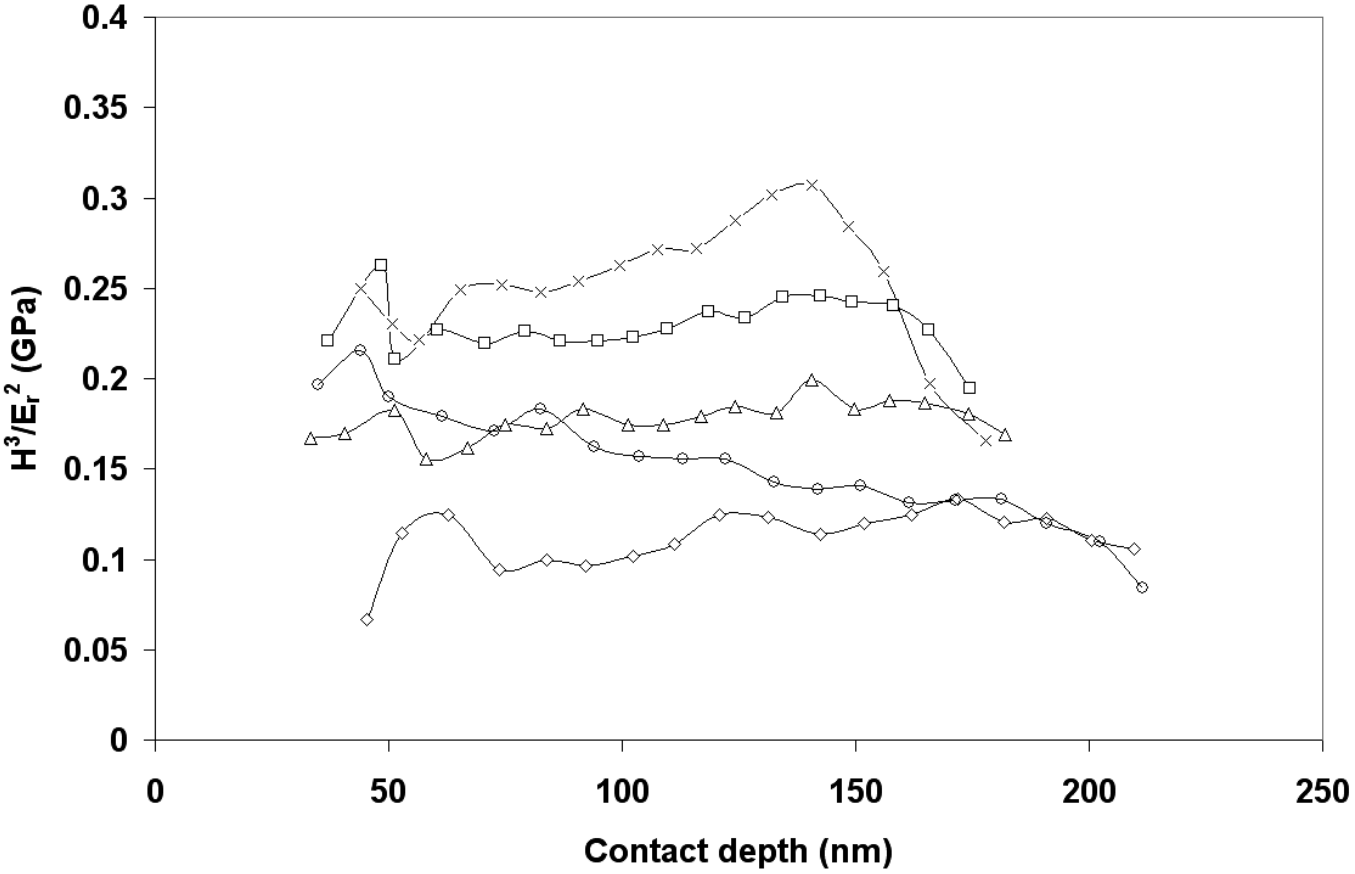

Figure 5 (fig 5 NEW.tif)

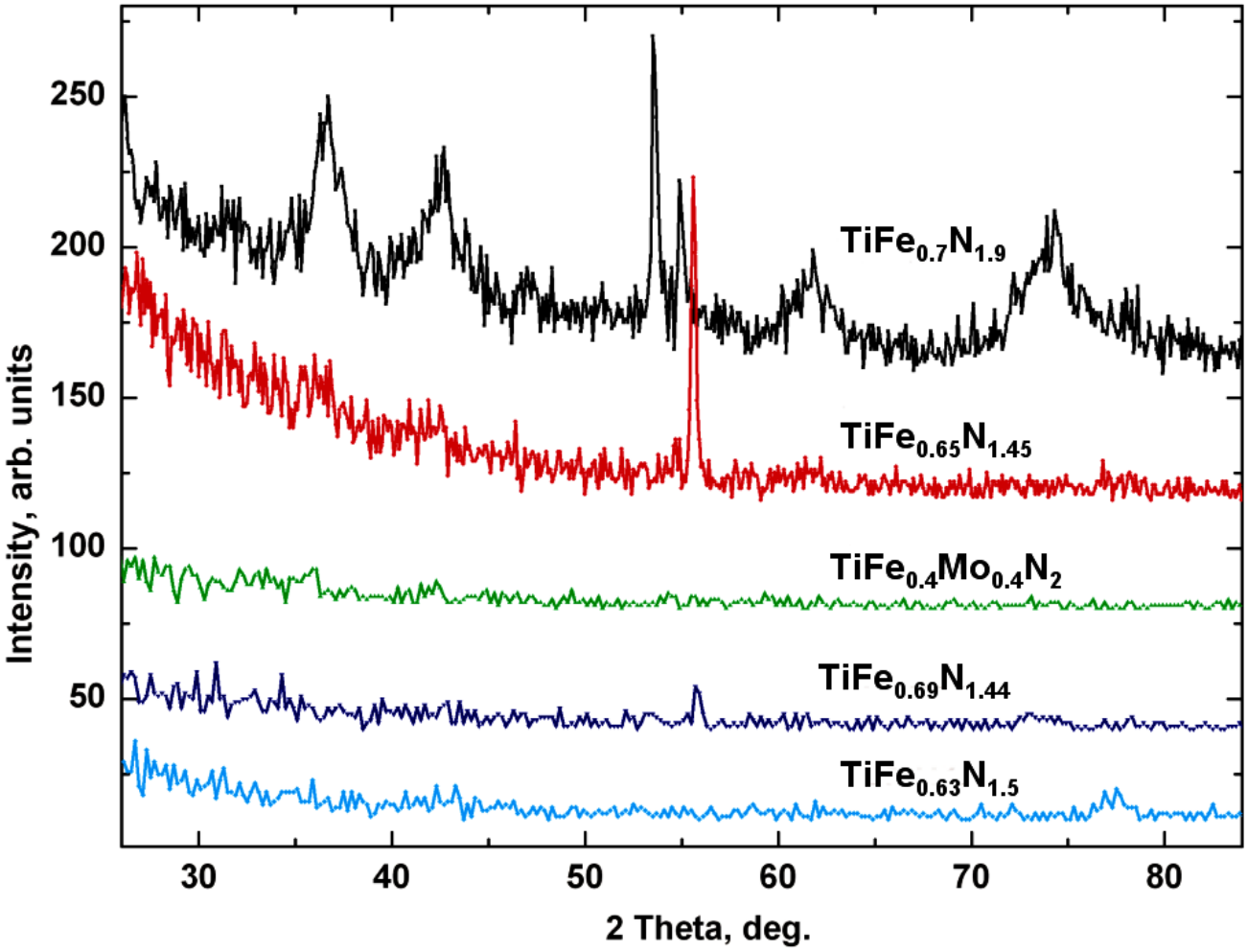

Figure 6 (Fig6.tif)